

## A DEPTH-AVERAGED 2-D SIMULATION FOR COASTAL BARRIER BREACHING PROCESSES

WEIMING WU<sup>1</sup>, NICHOLAS C. KRAUS<sup>2</sup>

1. *National Center for Computational Hydroscience and Engineering, The University of Mississippi, 346 Old Chemistry Building, University, MS 38677, USA. [wuwm@ncche.olemiss.edu](mailto:wuwm@ncche.olemiss.edu)*
2. *U.S. Army Engineer Research and Development Center, Coastal and Hydraulics Laboratory, 3909 Halls Ferry Road, Vicksburg, MS 39180, USA. [Nicholas.C.Kraus@usace.army.mil](mailto:Nicholas.C.Kraus@usace.army.mil)*

**Abstract:** A depth-averaged 2-D model has been developed for simulating coastal barrier breaching processes. The model solves the generalized shallow water equations and the non-equilibrium sediment transport and bed change equations in a coupled fashion using an explicit finite volume method on a rectangular grid. It considers interactions among transient flow, strong sediment transport, and rapid bed change by including bed change and variable flow density in the flow continuity and momentum equations. The model adopts the HLL approximate Riemann solver to handle the mixed-regime flows near the breach and the wetting-drying problem. The developed model has been tested against a lab experiment of dike-break flow over movable bed and a field experiment of sea dike breaching. The simulation results demonstrate that the model is capable of calculating the initial development stage of coastal barrier breaching under supercritical flow. Future work will improve the model to include waves for more general application in the coastal context.

### Introduction

Breaching often occurs on coastal barrier islands and spits, and at ephemeral river mouths and coastal lagoons and ponds either from the seaward side (Kraus et al. 2002) or from the bay side (Kraus et al. 2008) due to sustained high water level and wave overtopping. The main causes of breaching are overtopping flow and waves, as well as piping and seepage flows. Breaches can cause loss of human life, property, infrastructure, and transportation corridors; endanger navigation and stability of adjacent inlets; and degrade the environment by the exposure of bay perimeter to sea waves and by the change in bay salinity.

Coastal barrier and dike breach modeling has attracted more and more attention in recent years. Visser (1998), Kraus and Hayashi (2005) and D'Eliso (2007) developed simplified physically-based coastal barrier or dike breaching models, in which the breach cross-section is approximated as a trapezoid or rectangle, the overtopping flow is estimated using the broad-crested weir equation, the

Keulegan equation or the Bernoulli equation, and the breach morphological change is determined using simplified sediment transport models. Parkinson and Stretch (2007) investigated the temporal evolution of sand barrier breaching in estuaries and coastal lagoons based on laboratory experiments, and suggested a scaling method of breach formation time and peak outflow, considering the effects of outflow volume, hydraulic head, and barrier breadth. Roelvink et al. (2009) developed a depth-averaged 2-D model of coastal barrier breaching in which the shallow water equations with wave action and the non-equilibrium sediment transport equations are solved in a decoupled way using a finite difference method.

Wu et al. (2009) developed a depth-averaged 2-D numerical model for simulating the morphodynamic processes of earthen embankment breaching caused by overtopping flow. It uses a finite-volume shock-capture scheme based on the HLL approximate Riemann solver on rectangular mesh to handle the breach flow that is usually in mixed flow regimes and with discontinuities. It adopts a coupled solution algorithm, particularly considering the effects of strong sediment transport and rapid bed changes on the flow during the breaching process. This paper extends the model of Wu et al. to simulate the breaching processes of coastal barriers. The governing equations, numerical methods and validation of the developed model are presented in the next sections.

## **Governing Equations**

In comparison with dam and levee breaching in inland waters, coastal barrier and levee breaching processes are much more complex. The breaching can occur from either side of the barrier, and it is controlled by tidal flow, surge, wind and waves. A coastal barrier breach from the lagoon side usually opens rapidly and prevents wave penetration because of the ebb flow. An ephemeral ebb delta can also form. After water level in the bay drops and the exiting flow is reduced, waves can penetrate the breach at higher tide, causing a second rapid expansion of its width (Bokuniewicz et al. 2011). A breach from the sea side is often caused by storm surge and waves. The setup of water level by strong onshore-directed wind and surge during a storm and the run-up of waves contribute to the inundation, and the presence of waves in the incipient breach increases sediment mobilization and transport. A barrier breach may close naturally by the sediment transported from adjacent beaches and shores, or it can increase in size and become a new inlet or estuary (Kraus and Wamsley 2003).

To simplify the model formulation, this study focuses on the initial development stage under supercritical flow, which is the most critical stage of a coastal breach during overtopping flow. In this stage, the wave radiation stress,

turbulent stress, and Coriolis force are negligible in comparison with the inertia and gravitational forces. Because the breach opens rapidly, the interaction of flow, sediment transport and channel bed is significant; thus, the following generalized 2-D shallow water equations are herein used (Wu 2008):

$$\frac{\partial(\rho h)}{\partial t} + \frac{\partial(\rho u h)}{\partial x} + \frac{\partial(\rho v h)}{\partial y} + \rho_b \frac{\partial z_b}{\partial t} = 0 \quad (1)$$

$$\frac{\partial}{\partial t}(\rho u h) + \frac{\partial}{\partial x}(\rho u^2 h) + \frac{\partial}{\partial y}(\rho u v h) + \rho g h \frac{\partial z_s}{\partial x} + \frac{1}{2} g h^2 \frac{\partial \rho}{\partial x} + \rho g \frac{n^2 m_b u U}{h^{1/3}} = 0 \quad (2)$$

$$\frac{\partial}{\partial t}(\rho v h) + \frac{\partial}{\partial x}(\rho u v h) + \frac{\partial}{\partial y}(\rho v^2 h) + \rho g h \frac{\partial z_s}{\partial y} + \frac{1}{2} g h^2 \frac{\partial \rho}{\partial y} + \rho g \frac{n^2 m_b v U}{h^{1/3}} = 0 \quad (3)$$

where  $t$  is the time,  $x$  and  $y$  are the longitudinal and lateral coordinates,  $h$  is the flow depth,  $u$  and  $v$  are the flow velocities in  $x$  and  $y$  directions,  $U=(u^2+v^2)^{1/2}$ ,  $\partial z_b/\partial t$  denotes the rate of change in bed surface elevation,  $z_b$  is the bed surface elevation above a reference datum,  $z_s$  is the water level,  $n$  is the Manning roughness coefficient,  $g$  is the gravitational acceleration,  $\rho$  is the density of the water and sediment mixture in the water column determined by  $\rho=\rho_w(1-C_t)+\rho_s C_t$  with  $C_t$  being the volumetric concentration of total-load sediment,  $\rho_b$  is the density of the water and sediment mixture in the bed surface layer determined by  $\rho_b=\rho_w p'_m+\rho_s(1-p'_m)$  with  $p'_m$  being the porosity of the surface-layer bed material,  $\rho_w$  and  $\rho_s$  are the water and sediment densities, and  $m_b=[1+(\partial z_b/\partial x)^2+(\partial z_b/\partial y)^2]^{1/2}$  describes the effect of bed slope.

Simulation of the morphodynamic processes under barrier breach flow can be achieved by computing bed load and suspended load separately or the total load directly in the case of non-cohesive sediments. Here, the latter approach is taken, so that the sediment transport and bed deformation are determined with (Wu 2008)

$$\frac{\partial(hC_t)}{\partial t} + \frac{\partial(huC_t)}{\partial x} + \frac{\partial(hvC_t)}{\partial y} = -\frac{1}{L}(UhC_t - m_b q_{t*}) \quad (4)$$

$$(1-p'_m) \frac{\partial z_b}{\partial t} = \frac{1}{L}(UhC_t - m_b q_{t*}) \quad (5)$$

where  $q_{t*}$  is the total-load sediment transport capacity, and  $L$  is the non-equilibrium adaptation length of sediment transport. Note that the coefficient  $m_b$

in Eqs. (4) and (5) considers the lateral erosion along the side slope.  $L$  is given by

$$L = \max \left\{ L_b, \frac{Uh}{\alpha\omega_s} \right\} \quad (6)$$

where  $\omega_s$  is the settling velocity of sediment particles,  $L_b$  is the adaptation length of bed load, and  $\alpha$  is the adaptation coefficient of suspended load. Wu (2008) summarizes available methods to evaluate  $L_b$  and  $\alpha$  in the case of sediment transport under common flows; however, whether these methods are valid in the case of barrier breaching needs to be investigated.

The sediment transport capacity  $q_{t*}$  is determined using the formula of Wu et al. (2000), with the modification suggested by Wu (2008) to consider the effect of gravity on sediment transport over steep slope. In addition, to consider the effect of sediment concentration, the settling velocity  $\omega_s$  used in Wu et al. (2000) formula is determined by Richardson and Zaki's (1954) method:  $\omega_s = \omega_{s0}(1-C_t)^m$ , with  $m \approx 4.0$  and  $\omega_{s0}$  being the settling velocity of single sediment particles in quiescent, distilled water.

## Numerical Methods

The governing equations are solved with an explicit finite volume method on a non-staggered (collocated) rectangular grid system. The HLL approximate Riemann solver (Harten et al. 1983) is applied to determine the fluxes at cell faces. The water surface gradient is discretized by forward differencing if the velocity is positive and by backward differencing if the velocity is negative. The numerical method has first-order accuracy in both time and space. The sliding of loose materials along the two side walls of the breach is handled by the non-cohesive slope avalanching algorithm presented by Wu (2008). The flow and sediment transport equations are solved in a coupled fashion at each time step. Details of the numerical algorithm are discussed in Wu et al. (2009).

Because the above solution procedure is explicit, the computational time step should be limited by numerical stability conditions, such as the Courant-Friedrichs-Lewy (CFL) condition for flow computation and additional conditions for sediment transport and bed change computations. By trial and error, it was found that to obtain a stable solution, the bed change at each time step should be less than about 10% of the local flow depth. In this study, the time step length is determined by setting a Courant number of 0.25 and limiting

the ratio of bed change to local flow depth to be less than 0.1. This implies that the length of the time step varies during the simulation.

## Model Test

### *Case 1. Dike-Break Flow on Movable Bed in a Sudden-Expanded Channel*

Experiments of dike or dam break flow over a movable bed were conducted at the Civil Engineering Laboratory of the Université Catholique de Louvain (UCL), Belgium. The case selected to test the present model was performed in a 6 m long flume with a non-symmetrical sudden expansion from 0.25 m to 0.5 m in width, located 4 m downstream of the flume entrance (Fig. 1). The breaking of the dike was simulated by the rapid downward movement of a thin gate in the middle of the flume. The initial bed of the entire flume was covered by a 0.1 m thick horizontal layer of fully saturated sand, which was uniform coarse sand with a median diameter of 1.82 mm and specific gravity of 2.68, deposited with a porosity of 0.47. The initial water depth was 0.25 m on the upstream side of the gate and 0 m in the downstream side (Palumbo et al. 2008).

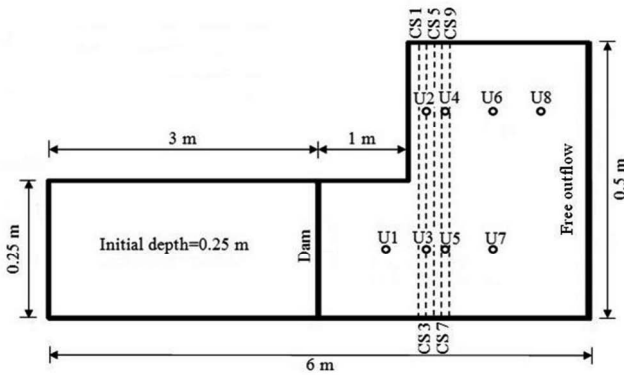


Fig. 1. Sketch of the UCL dike-break flow experiment setup (dashed lines and circles denote locations of measurement cross-sections and ultrasonic gauges, respectively).

The temporal evolution of the water level was measured by eight ultrasonic gauges placed downstream of the gate, as sketched in Fig. 1. The gauges U1, U3, U5, and U7 were aligned along a line 0.125 m away from the right flume wall (wall at bottom of Fig. 1) and located at 0.75, 1.2, 1.45, and 1.95 m downstream of the gate, respectively. The gauges U2, U4, U6, and U8 were aligned along a line 0.125 m away from the left wall (top wall in Fig. 1) and located at 1.2, 1.45, 1.95, and 2.45 m downstream of the gate, respectively. The morphological changes generated by the dike-break flow were measured at nine

cross-sections (numbered CS1 to CS9) located every 5 cm from 10 to 50 cm after the sudden expansion, at the end of the experiment by a laser sheet imaging technique.

The computational domain is represented by a mesh consisting of  $560 \times 100$  nodes in longitudinal and lateral directions. The longitudinal grid spacing is uniformly set as 0.005 m near the gate, but varies in the regions away from the gate. The lateral grid spacing is uniform and has a value of 0.005 m. The sediment adaptation length is determined by Eq. (6), with the suspended load adaptation coefficient  $\alpha$  equal to 4.0 and the bed load  $L_b$  set as 0.1 m. The time step length is determined by setting a Courant number of 0.25 and limiting the ratio of bed change to local flow depth to be less than 0.1. The Manning roughness coefficient is given as 0.025.

Fig. 2 shows the calculated total bed changes near the sudden expansion. One can see that erosion occurs near the corner of the expansion, and the eroded sediment deposits mostly at the expansion zone. Figs. 3(a)-(e) compare the measured and calculated final bed levels at five cross-sections: CS1, CS3, CS5, CS7 and CS9. At cross-sections CS1 and CS3, both the experiment and numerical model present erosion at the center of the flume near the corner of the sudden expansion, but the model underestimates the erosion along the expansion zone along the left flume wall and overestimates the erosion along the right wall. At cross-sections CS5, CS7, and CS9, the model reproduces well the bed profiles observed in the experiment. The deposition and erosion magnitudes and distributions are predicted with good accuracy.

Figs. 4(a)-(e) compare the measured and calculated water levels at gauges U1, U2, U3, U6 and U7. One can see that the model reproduces well the general trend of the dike-break wave propagation. On the five gauges, the root-mean-square error of the calculated water levels is 0.0089 m, and the correlation coefficient ( $R^2$ ) between the measured and calculated water levels is 0.92.

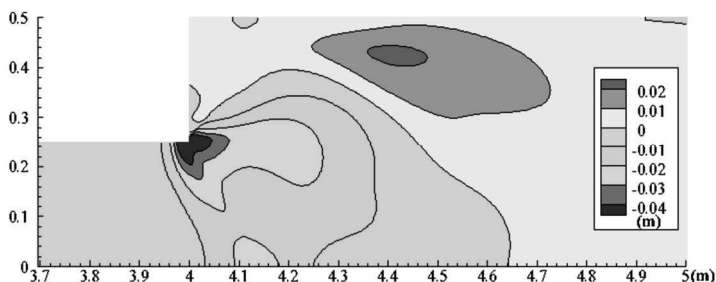


Fig. 2. Calculated total bed changes near the sudden expansion.

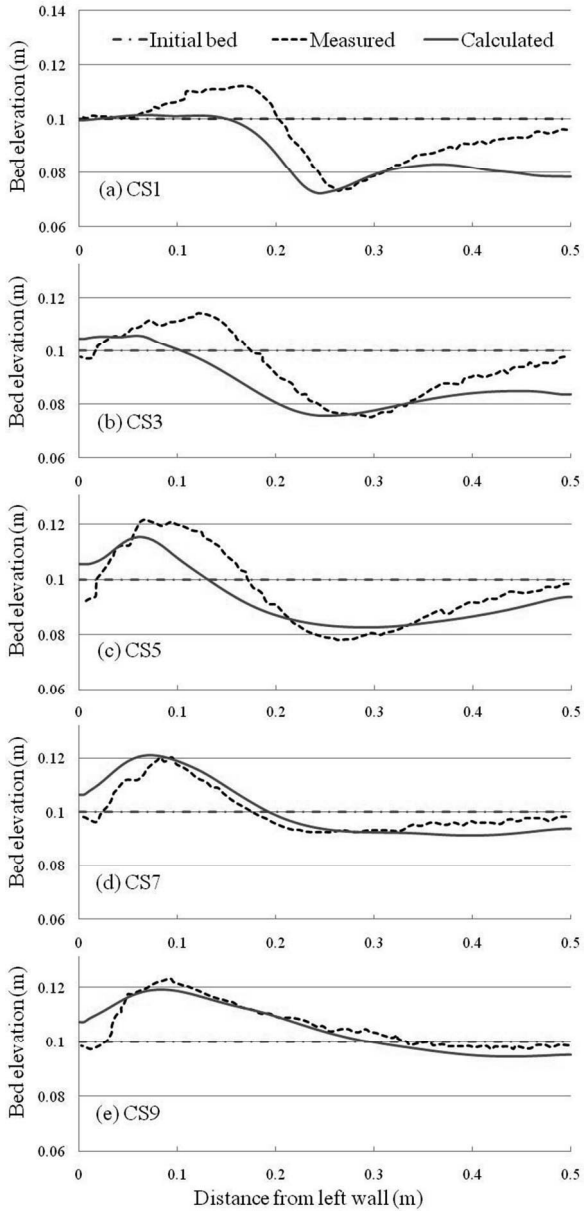


Fig. 3. Measured and calculated final bed levels at cross-sections CS1, CS3, CS5, CS7, and CS9.

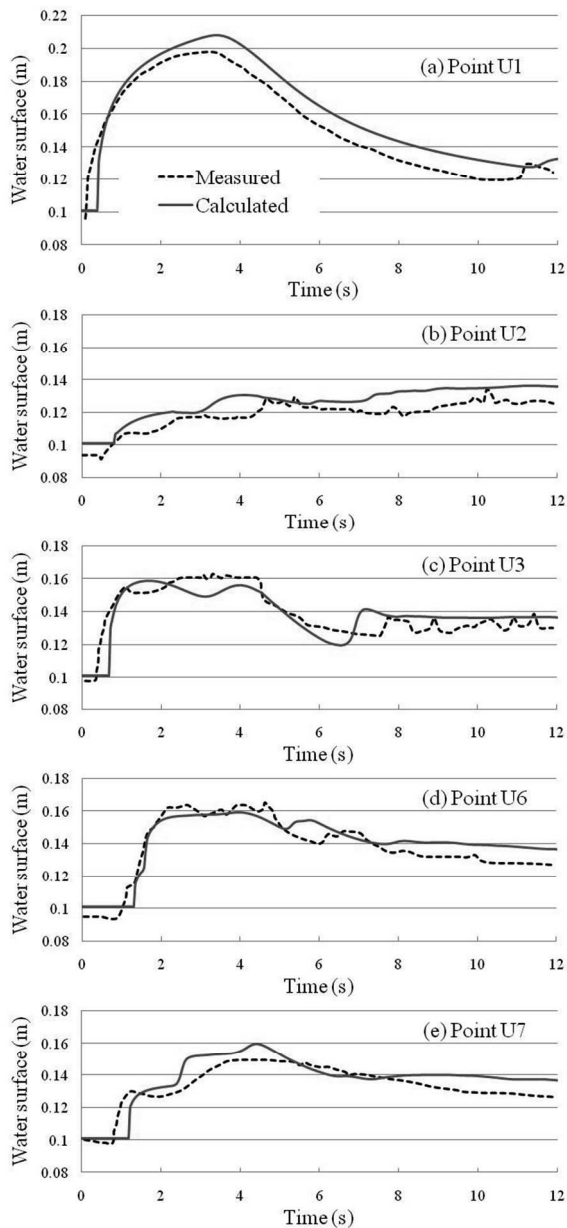


Fig. 4. Measured and calculated water levels at gauges U1, U2, U3, U6, and U7.

## *Case 2. Sea Dike Breaching in a Tidal Inlet*

The developed model has been further tested by comparison with the Zwin'94 field experiment measurements of sea dike breaching conducted at the Zwin Channel, a tidal inlet near the Dutch-Belgian border. The channel connects the nature reserve "Het Zwin" with the North Sea, and the reserve surface area is about  $1.5 \text{ km}^2$ , consisting largely of marshes and gullies. The mean tidal prism is about  $350,000 \text{ m}^3$ . A dike or barrier was built with local sand across the Zwin Channel, and its crest was 3.3 m above the mean sea level. Inclination of the outer slope (seaward side) was 1:1.6 and that of the inner slope (bay side) 1:3. The width of the crest was about 8.0 m. The bottom elevation of the Zwin Channel near its axis and outside the sand dike varied between 0.5 and 0.9 m, with an average of 0.7 m above the mean sea level. The dike sediments consisted of 'original' Zwin sand with a median diameter of 0.185 mm and additional sand with a median diameter of 0.315 mm transported alongshore from the Belgium coast. The initial breach had a depth of 0.8 m, and a width of about 1.0 m near its bottom or about 3.6 m near the crest of the dike. The tidal level outside the dike was measured during the breaching, and the highest water level was 0.27 m above the initial breach bottom. The experiment was done in quiet autumn weather with wind-speed of about 2 m/s and negligible wave height against the sand dike (Visser 1998).

The present study could not simulate the exact breach process because the topography in the polder area is not clear. Therefore, the simulation considers a hypothetical case with a sand dike with the same geometry and material as used in the experiment. The channel is approximated as a straight channel with a width of 60 m (about 20 m wider than the maximum breach width). The sand dike is located at 30 m from the inlet. The channel has approximately the same storage and surface area of the polder as those estimated by Smit and Snip (1995).

A mesh consisting of  $500 \times 200$  nodes in longitudinal and lateral directions is used in the simulation. The mesh is uniform near the sand dike, but nonuniform in the channel away from the dike. The grid spacing near the sand dike is 0.24 m in the longitudinal direction and 0.3 m in the lateral direction. The dike material porosity is estimated as 0.4. The sediment adaptation length  $L$  is calibrated as 2.0 m. A representative diameter of about 0.3 mm is specified for the sand in this simulation. The bed material repose angle is set to be  $32^\circ$ . The seaward side of the channel is set as an open boundary, with the water levels specified as the measured ones and the velocity copied from the adjacent internal nodes. A solid wall boundary condition is applied at the other end and along two banks of the channel.

Figs. 5(a)-(e) show the simulated flow pattern and bed topography at elapsed times of 1.5, 4, 8.5, 16, and 40 min after breaching, respectively. One can see the evolution of the breach with time. As the flow overtops the dike crest at the initial breach, erosion starts at the downstream (inner) slope and develops upstream, resulting in decrease of the width of the dike crest. As the bed is eroded vertically, the sediments on the two side walls of the breach slide at the repose angle and the breach is widened gradually. A large scour hole appears at the center of the channel near the breach, while the eroded sediments are transported by the flow and immediately deposited along the sides and downstream edge of the scour hole. The numerical model gives an intuitively reasonable general flow pattern and change in depth contours near the breach. The model produces antidunes or standing waves on the bottom at the early stage of breaching with supercritical flow, and these disappear at the end of breaching after the flow reduces and becomes subcritical.

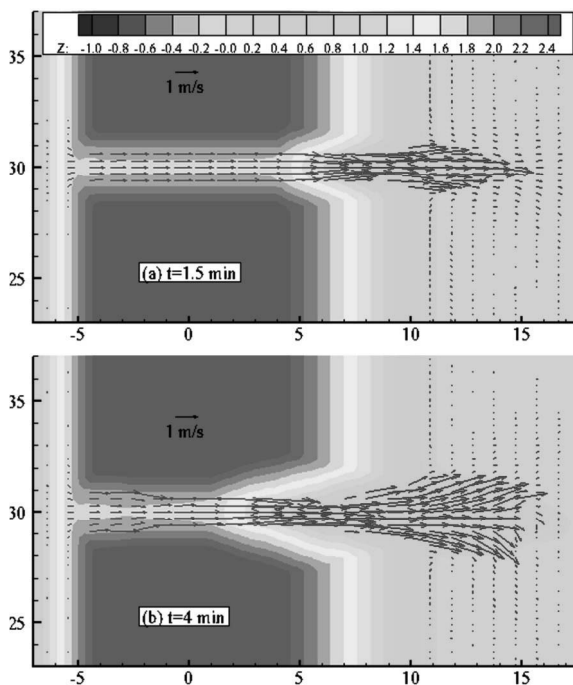


Fig. 5. Simulated flow pattern and breach topography (background as bed elevation contours in meter; x and y coordinates in meter).

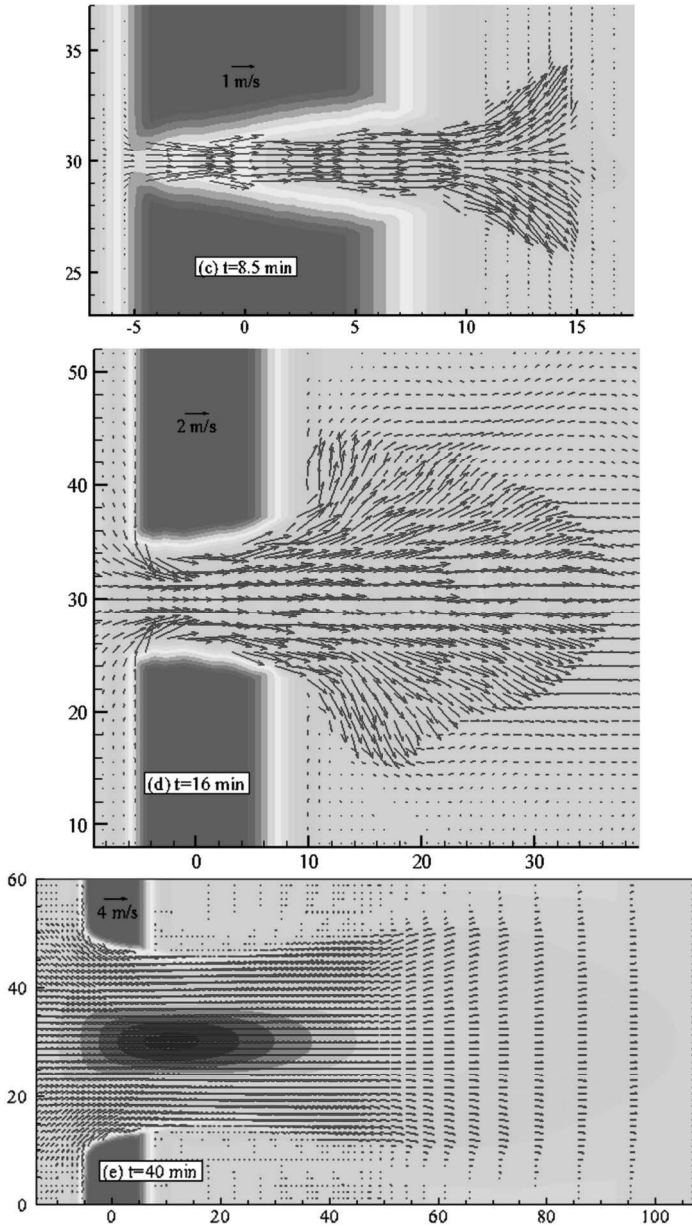


Fig. 5 (cont'd). Simulated flow pattern and breach topography (background as bed elevation contours in meter; x and y coordinates in meter).

Fig. 6 compares the measured and simulated breach widths. The breach width starts to increase significantly after  $t=5.5$  min but increases slowly after about 35 min. The breaching process finishes at about 53 min when the water level in the bay rises to approximately the same as the tidal level outside the sand dike. The measured breach width at 60 min is 41 m, while the simulated one is 40.5 m. The simulation results agree generally well with the measurements

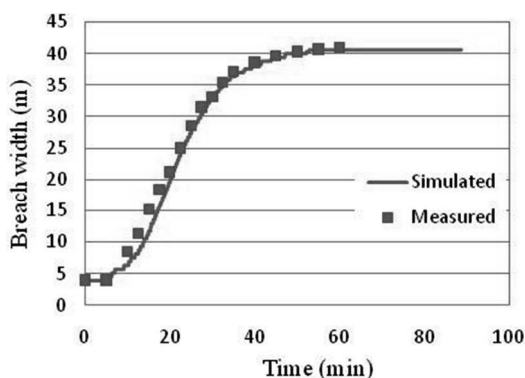


Fig. 6. Comparison of measured and simulated breach widths.

## Conclusions

A depth-averaged 2-D finite-volume model was established to simulate the coastal barrier breaching processes accompanying overtopping flows. The effects of sediment concentration and bed change on the flow are represented in the continuity and momentum equations. The sediment transport model simulates the non-equilibrium transport of total load. An explicit algorithm based on the finite volume method is adopted to solve flow, sediment transport, and bed change equations. The model adopts the HLL approximate Riemann solver to describe the mixed-regime flows near the breach. To enhance the performance of the model, a varying time step is implemented that satisfies the CFL condition and ensures the bed change at each time step is less than ten percent of the local flow depth.

The developed model was tested using a laboratory experiment of dike-break flow on a movable bed carried out at the Université Catholique de Louvain, and a field experiment of sea dike breaching conducted at the Zwin Channel, which is a tidal inlet near the Dutch-Belgian border. The model overall predicts well the breach width and the flow pattern near the breach. The model simulates that antidunes or standing waves appear in the early stage of breaching with

supercritical flow, and they disappear at the end of breaching when the flow becomes subcritical. Replication of these processes implies that the model is capable of simulating the initial (catastrophic) developmental stage of a breach, when its depth and width change rapidly under supercritical flow. To better represent the complex breaching of barrier and dike in the coastal context, the model will be enhanced in the near future to take into account the effect of waves.

### Acknowledgements

Dr. Julie D. Rosati is acknowledged for her comments and suggestions to improve this paper. Mr. Reza Marsooli is thanked for his help in model testing. This work was supported by the Coastal Inlets Research Program, U.S. Army Corps of Engineers (USACE). Permission was granted by Headquarters, USACE, to publish this information.

### References

- Bokuniewicz, H.J., Kraus, N.C., Munger, S., Slattery, M., Coffey, R. (2011) "Monitoring incipient breaching at an artificial inlet: Georgica Pond, New York," Proceedings, Symposium to Honor Dr. Nicholas C. Kraus, *J of Coastal Res.*, Special Issue, No. 59, ISSN 0729-0208.
- D'Eliso, C. (2007). "Breaching of sea dikes initiated by wave overtopping: A tiered and modular modeling approach," Ph.D. Dissertation, University of Braunschweig, Germany and University of Florence, Italy.
- Harten, A., Lax, P.D., and van Leer, B. (1983). "On upstream differencing and Godunov-type schemes for hyperbolic conservation laws," *SIAM Review*, 25(1), 35–61.
- Kraus, N.C., and Hayashi, K. (2005). "Numerical morphologic model of barrier island breaching." *Proc. 29th Coastal Eng. Conf.*, World Scientific Press, pp. 2120-2132.
- Kraus, N.C., Patsch, K., and Munger, S. (2008). "Barrier beach breaching from the lagoon side, with reference to Northern California," *Shore & Beach*, 76(2): 33-43
- Kraus, N.C., Militello, A., and Todoroff, G. (2002). "Barrier breaching processes and barrier spit breach, Stone Lagoon, California," *Shore & Beach* 70(4): 21-28.

- Kraus, N.C., and Wamsley, T.V. (2003). "Coastal barrier breaching, Part 1: Overview of breaching processes," Coastal and Hydraulics Engineering Technical Note ERDC/CHL CHETN-IV-56, U.S. Army Engineer Research and Development Center, Vicksburg, MS.
- Parkinson, M., and Stretch, D. (2007). "Breaching timescales and peak outflows for perched, temporary open estuaries," *Coastal Engineering Journal*, World Scientific Publishing Company and Japanese Society of Civil Engineers, 49(3), 267–290.
- Palumbo, A., Soares-Fraza, S., Goutiere, L., Pianese, D., and Zech, Y. (2008). "Dam-break flow on mobile bed in a channel with a sudden enlargement," *River Flow 2008*, Turkey, pp. 645-654.
- Richardson, J. F., and Zaki, W. N. (1954). "Sedimentation and fluidisation, part I," *Trans., Inst. Chem. Engrs.*, 32(1), 35–53.
- Roelvink, D., Reniers, A., van Dongeren, A., de Vries, J.v.T., McCall, R., and Lescinski, J. (2009). "Modelling storm impacts on beaches, dunes and barrier islands," *J. Coastal Eng.*, Elsevier, 56, 1133–1152.
- Smit, M.J., and Snip, D.W. (1995). "Preparation of Zwin'94 experiment. Part I: theoretical investigation," M.Sc. Thesis, Delft University of Technology, Delft, The Netherlands (in Dutch).
- Visser, P.J. (1998). "Breach growth in sand-dikes," *Communications on Hydraulic and Geotechnical Eng.*, Report No. 98-1, Delft University of Technology, The Netherlands.
- Wu, W. (2008). "*Computational River Dynamics*," Taylor & Francis, UK.
- Wu, W., He, Z., and Wang, S.S.Y. (2009). "A depth-averaged 2-D model of non-cohesive dam/levee breach processes," *Proc. 2009 World Environmental and Water Resources Congress*, May 17-21, Kansas City, MO (on CD-Rom).
- Wu, W., Wang, S. S. Y., and Jia, Y. (2000). "Nonuniform sediment transport in alluvial rivers," *J. Hydraulic Res.*, IAHR, 38(6), 427–434.